2023, 20(3 Suppl.): 1064 - 1077
https://dx.doi.org/10.21123/bsj.2023.8476
P-ISSN: 2078-8665 - E-ISSN: 2411-7986
Baghdad Science Journal

Visible-Light-driven Photocatalytic Properties of Copper(I) Oxide (Cu_2O) and Its Graphene-based Nanocomposites

Abdul Waheed Rabbani*[1], Gul Naz[1], Elyor Berdimurodov[2], Basant Lal[3], Aigul Baimagambetova Sailauovna[4] and Ahmad Hosseini-Bandegharaei*[5]

[1]Institute of Physics, The Islamia University of Bahawalpur, Bahawalpur 63100, Pakistan.
[2]Faculty of Chemistry, National University of Uzbekistan, Tashkent, Uzbekistan
[3]Department of Chemistry, Institute of Applied Science and Humanities, GLA University, Mathura-281406, India
[4]Institute of Natural Sciences and Geography, Abai University, Almaty 050010, Kazakhstan
[5]Faculty of Chemistry, Semnan University, Semnan, Iran
*Corresponding Author.

Received 28/01/2023, Revised 02/05/2023, Accepted 04/05/2023, Published 20/06/2023

Abstract

In this study, an improved process was proposed for the synthesis of structure-controlled Cu2O nanoparticles, using a simplified wet chemical method at room temperature. A chemical solution route was established to synthesize Cu2O crystals with various sizes and morphologies. The structure, morphology, and optical properties of Cu2O nanoparticles were analyzed by X-ray diffraction, SEM (scanning electron microscope), and UV-Vis spectroscopy. By adjusting the aqueous mixture solutions of NaOH and NH2OH•HCl, the synthesis of Cu2O crystals with different morphology and size could be realized. Strangely, it was found that the change in the ratio of de-ionized water and NaOH aqueous solution led to the synthesis of Cu2O crystals of different sizes, while the morphology of Cu2O crystals was not affected. The synthesized Cu2O crystal samples were used as photocatalysts for methyl orange (MO) dye decomposition, as a model molecule, to evaluate the photocatalytic activities. However, under 200 watts of a visible light source, there are four samples with and without graphene-based nanocomposite of Cu2O NPs. The results showed that, compared with roughly spherical, irregular but thick plates, brick and small granule spheres shaped Cu2O nanoparticles provided better activity. The Cu2O sample with irregular but thick platelet-like shapes, having an average particle size of 0.53 µm, exhibited excellent photocatalytic activity (99.08% degradation). In addition, by reducing the size of Cu2O particles and preparing their graphene composition, one can fabricate a sample (Cu2-Cu2Gr) with the highest efficiency which has significantly better photocatalytic activity in comparison to the others. This work represents an innovative strategy for pre-the-case production of nanomaterials with shapes and sizes, that is, Cu2O crystals, with excellent photocatalytic activity through compositing with graphene.

Keywords: Cu_2O, Graphene-based nanocomposites, Nanocrystals, Photocatalytic evaluation, Visible-Light

Introduction

In the past few years, mastering the tunable structure of inorganic nano-materials to find new properties has become one of the main goals of nanoscience and technology [1]. Such types of nanomaterials have size-dependent optical, electronic, magnetic, chemical, and mechanical properties that are not available in their bulky counterparts [2]. Due to its special characteristics, including its capacity to accelerate chemical processes in the presence of light, and its ban gap being in the visible spectrum, having a shortfall in electrons and holes, and having high stability, Cu_2O is a very alluring metal oxide semiconductor[3]. As an important type of semiconductor with a band gap of 2.17 eV [4], Cu_2O has been widely used in catalysis [5], magnetic storage media [6], solar cells [7], dyes photodegradation [8], lithium-ion battery electrodes [9], and gas sensors [10]. In fact, the size, shape, and form of the nanoparticles have a significant impact on their attributes and activities[11]. Among all metal oxides, copper oxide nanomaterials have received more attention due to their unique properties [12]. Although there are several methods to synthesize Cu_2O nanostructures [13], the chemical reduction method is a more convenient way to synthesize copper nanoparticles, by changing experimental parameters such as temperature, concentration, pH, *etc.* [14]. This method not only produces a large number of nano-products in a short period but also leads to a high-quality structure which enhances the nano-product performance [15]. The main disadvantage of the synthesis of Cu_2O nanoparticles by the reduction method is the stability of the acquired nanoparticles [16]. When prepared in an aqueous medium, the newly formed Cu_2O nanoparticles will be oxidized under ambient conditions regardless of the nature of the reducing agent used [17].

As aforementioned, it is well known that the shape and size of inorganic materials have a great influence on their physicochemical properties. The synthesis of Cu_2O nanostructures is becoming more and more attractive due to the relatively easy preparation, low cost, and wide range of potential applications [18]. In recent years, scientists have made a lot of efforts in the synthesis of Cu_2O nanomaterials with different shapes, such as nanorods [19], nanowires, nanobelts [20], octahedrons [3], etc. However, how to effectively achieve the controlled synthesis of materials with the required shape and size remains a huge challenge. Emphasizing the use of Cu_2O nanoparticles, it is possible to have more understanding of the photocatalytic properties of Cu_2O, which can be provided by consuming these nanocrystals with a certain shape [5, 21].

Graphene is an advantageous substance with sp^2-hybrid carbon, which has also been introduced into science, medicine, and engineering circles [22]. In 2004, this visual material was produced for the first time during the electro-exfoliation process. In addition to adopting carbon doping for preparation of materials with smaller bandgap, composition formation with graphene nanosheets also increase the light absorption rate of semiconductor-graphene-based NPs. Graphene used as a photosensitizer further expands the fascination with visible light and also increases the photolysis of terminal semiconductor contaminants [23]. The effective compensation of photogenerated electron-hole pairs can reduce energy-ineffective electron-hole recombination [24]. The liquefied mixture of $CuCl_2$, SDS, NaOH, and $NH_2OH{\cdot}HCl$ is arranged to prepare these nanosubstances at room temperature. Cu_2O rhombohedral dodecahedrons show exceptionally high-quality photocatalytic activity.

In this study, the synthesis and photocatalytic activity of Cu_2O and Cu_2O/graphene were scrutinized. In graphene-based composites, due to the adsorption of dyes on the graphene surface and the easy transfer of electrons to the metal oxide conduction band, the photocatalytic activity is significantly enhanced in the graphene-based Cu_2O heterojunction composite. However, despite its huge potential, the photocatalytic efficiency of pristine graphene is still very fast due to the rapid recombination of photogenerated electron-hole pairs in single-phase semiconductors. Therefore, the composition of Cu_2O can lead to the preparation of a more outstanding photocatalyst. As far as we know, no early reports have been made on the comparison of the photocatalytic activity of Cu_2O and its composition with graphene. Therefore, this research was designed to afford such a comparison.

Materials and Methods

Experimental Work

Materials

Substances for the subsequent synthesis of Cu_2O nanoparticles include copper chloride ($CuCl_2$; Sigma-Aldrich, 99.0%), sodium hydroxide (NaOH; Sigma-Aldrich, 98%), sodium lauryl sulfate (SDS surfactant; Sigma-Aldrich, 90%), hydroxylamine ($NH_2OH{\cdot}HCl$; reducing agent; Sigma-Aldrich, 99%), methyl orange (MO; Sigma-Aldrich, 99%), deionized H_2O (as Solvent), and acetone (Sigma-Aldrich). All these synthetic chemicals were purchased from Sigma Aldrich and exploited without further purification. TR-rGO powder was purchased from Alibaba.com from China.

2023, 20(3 Suppl.): 1064 - 1077
https://dx.doi.org/10.21123/bsj.2023.8476
P-ISSN: 2078-8665 - E-ISSN: 2411-7986
Baghdad Science Journal

Instrumentation

The phase purity and crystal structure of the prepared samples were examined by X-ray diffraction (XRD) recorded on a D8 Advance X-ray diffraction (Bruker, Germany) with a Cu anode as an X-ray source, employing a scanning rate of 0.02° /second in the 2θ range of 20° to 80°. The machine was operated at 40 kV and 35 mA with a radiation source of Cu Kα λ = 0.15418 nm. Scanning electron micrograph (SEM) images were obtained using a field emission SEM (FESEM) instrument (Hitachi S-4800 II, Japan) and TEM was used to analyze molecule levels for rGO samples using Philips EM120 TEM instrument operating at an accelerating voltage of 80 kV. The UV-Vis absorbance spectroscopy apparatus (Cecil Instruments - Cecil 7400 Double Beam UV/VIS Spectrophotometer, Aquarius Company with wavelength 190 nm-1100 nm).

Synthesis of Cu_2O Nanostructures

Cu_2O nanocrystals with different structures are mostly prepared by wet-chemical, electrodeposition, and solvothermal production methods [25]. However, in this project, the wet-chemical production method was applied to producing Cu_2O nanocrystals to obtain tunable structures. Firstly, for the synthesis of Cu_2O nanocrystals, stock solutions of all chemicals were prepared before mixing the given ingredients. For this purpose, all-glass vials were washed amid detergent, and standard de-ionized water and finally rinsed through acetone. As the amounts of exploited regents have been given in Table 1. Firstly, for the production of Cu_2O nanocrystals with dissimilar morphologies, 9.0 mL, 8.95 mL, 8.90 mL, and 8.85 mL of de-ionized water were added to four glass beakers labelled with 1, 2, 3, and 4, respectively. Afterwards, 0.1 mL of 0.1 M $CuCl_2$ solution was added to each of the four different labelled beakers. The reaction mixture was stirred continuously at room temperature for 3 minutes to make a homogeneous solution. After stirring for about 5 minutes, 0.20 mL, 0.25 mL, 0.30 mL, and 0.35 mL of 1.0 M NaOH (as given in Table 1**.** were poured into different glass beakers of 1, 2, 3, and 4, respectively. The beakers were stirred again for another 5 minutes. After that, 89 mg of SDS were added to the labelled beakers one by one, and further continuous stirring was continued at room temperature until the powder was completely dissolved.

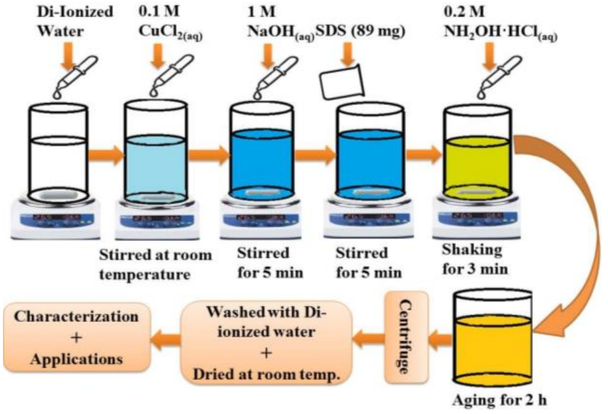

Figure 1. Demonstration of the preparation of Cu_2O NPs with different concentrations of DI-H_2O, $CuCl_2$, NaOH, SDS, and $NH_2OH{\bullet}HCl$ in a mixed aqueous solution.

When SDS was completely dissolved in all four beakers, 0.70 mL of 0.2 M $NH_2OH{\cdot}HCl$ was mixed with all these solutions and stirred at room temperature for 3 minutes. After shaking the solutions, the four samples were immediately covered with high-quality aluminum foil and kept in the cabinet for 2 hours to obtain the required Cu_2O nanocrystal products with various morphologies. The total volume of the solution in each beaker was 10 mL, and its colour changed from blue to orange and then to pale yellow during the process. Various Cu_2O nanoparticles with different structures were prepared by using different chemical solutions containing pre-specified concentrations of reagent (Fig 1), summarized in Table 1.

Table 1. Various concentrations of the reagents were used to prepare different Cu_2O nanostructures.

Sample ID	H_2O (DI) mL	$CuCl_2$ (0.1 M) mL	NaOH (1 M) mL	SDS) (mg)	$NH_2OH{\cdot}HCl$ (0.2 M) mL	Total Volume of Sample (mL)
Cu_1	9.0	0.10	0.20	89	0.70	10
Cu_2	8.95	0.10	0.25	89	0.70	10
Cu_3	8.90	0.10	0.30	89	0.70	10
Cu_4	8.85	0.10	0.35	89	0.70	10

2023, 20(3 Suppl.): 1064 - 1077
https://dx.doi.org/10.21123/bsj.2023.8476
P-ISSN: 2078-8665 - E-ISSN: 2411-7986
Baghdad Science Journal

Preparation of Cu_2O/rGO Nanocomposites

Various nanocomposites were constructed with a Cu_2O/rGO ratio of 6:3 (w/w). For these syntheses, 90 mg of Cu_2O and 45 mg of rGO were poured in two different beakers containing 50 ml of doubly distilled water and sonicated for 30 minutes. The homogenized suspensions of rGO and Cu_2O were mixed and further agitated with ultrasonic wave for 60 minutes. Eventually, the acquired suspensions of Cu_2O/rGO were oven- dried and exploited for photocatalytic system.

Evaluation of Photocatalytic Performance under Visible Light Irradiation

The photocatalytic activity of the prepared Cu_2O samples on the degradation of methyl orange (MO) dye solution was evaluated under visible light irradiation. A 200-watt visible lamp was utilized as the light source to provide visible light illumination. All experiments were performed in air at room temperature. Cu_2O/rGO composite was constructed with a Cu_2O/rGO ratio of 6:3 (w/w). In each experiment, 10 mg of photocatalyst powder (bare Cu_2O or Cu_2O/rGO composite) was added to 50 mL of MO solution (0.03 mM). Before irradiation, the suspension was magnetically stirred in the dark for 30 minutes to allow MO to reach adsorption-desorption equilibrium on the catalyst surface and then exposed to visible light irradiation. While stirring the sample under visible light, 3 mL of the suspension was collected every 10 minutes and filtered to remove catalyst nanoparticles. The MO solution without a catalyst was then analyzed using a UV-Vis spectrophotometer.

Results and discussion

Structure and Morphology

To check the structure and size of the nanocrystals in these four Cu_2O samples, X-ray diffraction of the deposit was recorded for each sample. Fig 2 shows the obtained X-ray diffraction arrangements which display that the peak positions at 2θ (degree) angles are equal to (110), (111), (200), (211), (221), (220), (310), (3111) and (222) lattice plane. All these peaks originated from copper(I) NPs which were fabricated with different H_2O: NaOH ratios. Due to the change in the ratio of H_2O: NaOH, the (111) peak intensity of samples Cu_1 to Cu_3 increases, while the (200) peak intensity decreases. Since the elongated nanostructures show more intense (111) planes [26], increases in (111) peak intensity from samples Cu_1 to Cu_3 and the simultaneous decrease in (200) peak intensity reveals that from samples Cu_1 to Cu_3 the dimensions of Cu_2O nanoparticles becomes greater. Nevertheless, in sample Cu_4 again the peak intensity of the (111) plane decreases, as the peak intensities in Fig 2. exhibited.

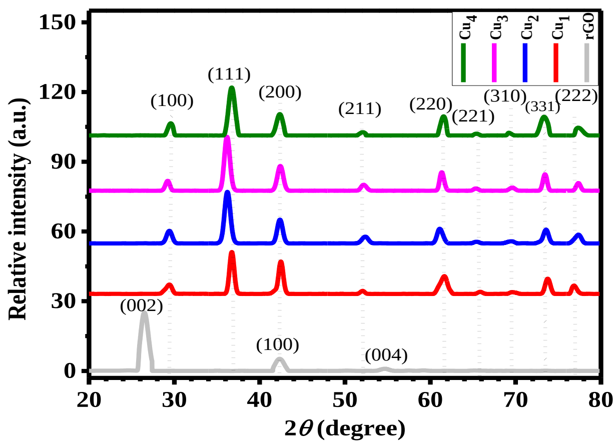

Figure 1. The XRD sketches of rGO and four Cu_2O NPs

The peak intensity of the prepared Cu_2O samples with different concentrations of deionized water and NaOH decreased significantly from sample Cu_1 to sample Cu_2. This means that when the meditation of NaOH increases, the peak intensity in the XRD decreases steadily, and the (211) diffraction peak in the XRD pattern almost disappears. Therefore, the deposited samples with different amounts of NaOH showed dramatic variations in the crystallinity and structure of Cu_2O [27]. The results showed that NaOH has an extraordinary effect on the surface morphology of Cu_2O samples, which indicates that the shape of the interface is affected by the concentration of NaOH in this process. This reflection, which is different from the transition, is caused by the consistency of the particle shape. Due to the nanosize effect, some peak widths are

2023, 20(3 Suppl.): 1064 - 1077
https://dx.doi.org/10.21123/bsj.2023.8476
P-ISSN: 2078-8665 - E-ISSN: 2411-7986
Baghdad Science Journal

observed. Since the peak intensity of XRD becomes irrelevant to the size of the NP of 150 nm or more, the sample Cu_1 exhibits sharp (111) peak and (200) peak intensities due to the high single-crystallization rate. Compared with all other samples, the intensity of the (111) peak is higher in Cu_2. This indicates that compared with the (111) peak of other samples, 0.25mL NaOH solution is more suitable for the high-intensity growth on the (111) surface. However, the intensity of the (111) peak in samples Cu_2 and Cu_3 are similar, but in Cu_1, the (220) peak is more prominent, which indicates that the surface morphology of the nanostructure has undergone tremendous changes. Compared with the sample Cu_2/Cu_3 with the same growth but lower intensity, sample Cu_1 has fewer planes (111). Similar to Cu_1, sample Cu_4 has the highest intensity in the (311) peak compared with all other samples.

The (110) characterization peak of Cu_2O NPs in all four samples are observed at almost 2θ =29.30, while the prominent peak of all samples is observed around about 36.55. The crystallite size of these four Cu_2O nanoparticles was calculated by using the Debye-Scherrer relation (Eq1. $D= K\lambda/ \beta cos\theta$)

In this equation, "D" is crystallite size, "K" is Sherrer constant and equal to 0.9, "λ" is the wavelength of X-rays used during the experiment and corresponded to CuKα 1.5406 Å, "θ" is Bragg's angle while "β" is full width at half maxima (FWHM) [28]. The results obtained from the Scherrer equation and the average crystallite sizes calculated by the method discussed below are summarized as follows in Table 2.

The reduction in the size of the nanocomposite crystallites shows a larger surface-to-volume ratio. When sunlight is irradiated, more light-excited electron-hole pairs are generated and their photocatalytic activity is enhanced. Measuring the dislocation density due to crystal defects was performed by using the formula $\delta =1/D^2$ [28], and the calculated values are listed in Table 2. The dislocation density (δ) increases as the crystallite size decreases, and vice versa. Significant changes were found through the strains in the four Cu_2O, which changed from tensile strains in the nanoparticles to compressive strains. This change in microstrain may be due to the changes in the structure, crystallite size, and morphology, given in Table 2. Therefore, in all four samples, the intensity of the (111) surface is more prominent than that of the Cu_2 sample, which has more photocatalytic activity and, the result is given in Table 3. With 90.01% photodegradation of MO (Table 3), it proved that is the best photocatalyst.

Table 2. Average crystallite size, lattice strain, dislocation density, and lattice spacing calculated from the Debye Scherrer method.

Samples name	Average crystallite size D(nm)	lattice spacing d (Å)	Dislocation density δ $(nm)^{-2}$	Strain ε
Cu_1	**13.15**	**0.1794**	**0.0071**	**0.1591**
Cu_2	**11.67**	**0.1798**	**0.0075**	**0.1717**
Cu_3	**14.17**	**0.1798**	**0.0054**	**0.1444**
Cu_4	**12.29**	**0.1788**	**0.0067**	**0.1625**
rGO	**7.06**	**0.2483**	**0.0200**	**0.2483**

SEM Analysis

It is observed from the SEM image that these four samples show various structures. The Cu_1 sample is roughly spherical with an average elongation of 2.77 µm. Sample Cu_2 has an irregular but thick plate-like shape with an average particle size of 0.53 µm. Cu_3 looks like a brick with a maximum average particle size of 4.22 µm, which shows more elongation in the nanocrystalline structure. Among the Cu_4 nanoparticles, they are small particles that appear in clusters. The average particle size cannot be measured, but the estimated size is less than 100 nm. The Cu_4 sample has a powder structure composed of small crystal grains, and the structure is agglomerated due to improper/fine pulverization of the dried sample. There is elongation from Cu_2 to Cu_3, and it is confirmed by XRD that the (111) peak intensity increases but the (200) peak intensity decreases.

2023, 20(3 Suppl.): 1064 - 1077
https://dx.doi.org/10.21123/bsj.2023.8476
P-ISSN: 2078-8665 - E-ISSN: 2411-7986

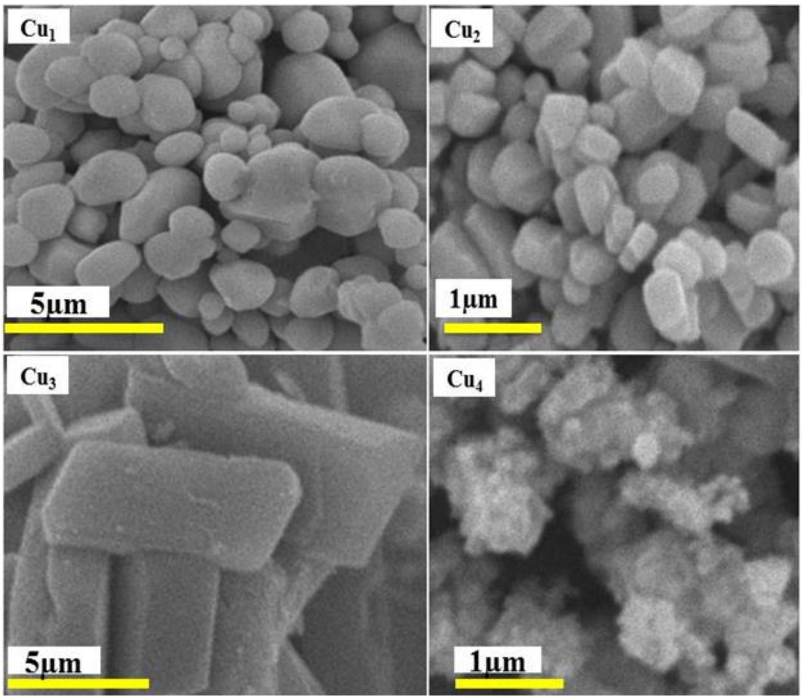

Figure 3. SEM images of samples Cu_1, Cu_2, Cu_3, and Cu_4 prepared at different concentrations of deionized water and NaOH.

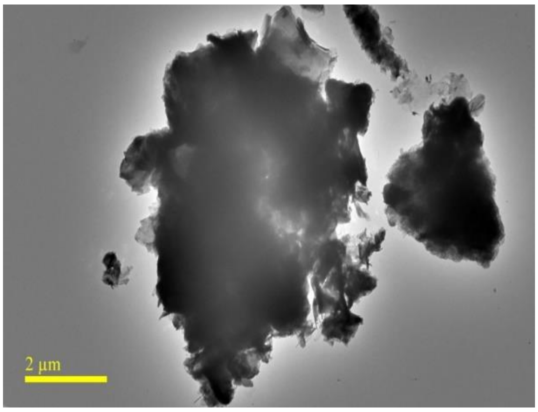

Figure 4. TEM images of reduced graphene (rGO).

For achieving, better performance of Cu nanoparticles used rGO and rGO have a humidity sensor and a large surface area to volume ratio (displayed in TEM image; Fig 4), high vacancy density, and hydrophilic functional group on the surface of rGO, which creates new water molecules, that are easily adsorbed on the material surface and thus improves the response of the sensor. Furthermore, the special structure of rGO/Cu allows the charge to transfer from water to Cu nanoparticles, thereby increasing conductivity.

Optical Properties

The spectral analysis of Cu_2O nanoparticles is carried out by using UV-Vis absorption spectra with a wavelength of 190 nm-1100 nm. Fig 5 shows the results of the UV-Vis absorption spectra of samples Cu_1, Cu_2, Cu_3, and Cu_4. It was observed that the ratio of DI-H_2O: NaOH in the reaction solution strongly affected the grain size of the nanoparticles (shown in XRD patterns; Fig 2 and the morphological size of the nanoparticles (shown in SEM micrographs; Fig 3 . One can calculate the band gap of the Cu_2O products by using the converted Kubelka-Munk function versus the energy of the excitation light [29]. The peak positions of samples Cu_1, Cu_2, Cu_3, and Cu_4 appear at 655 nm, 517 nm, 600 nm, and 511 nm, and the measured energy gaps are in the range of 2.12 eV to 2.24 eV, given in Fig 6. Hence, it is revealed that the change in the ratio of DI-H_2O:NaOH in the reaction solution causes a significant change in the peak position, that is, it causes the color shift of the absorption peak.

2023, 20(3 Suppl.): 1064 - 1077
https://dx.doi.org/10.21123/bsj.2023.8476
P-ISSN: 2078-8665 - E-ISSN: 2411-7986

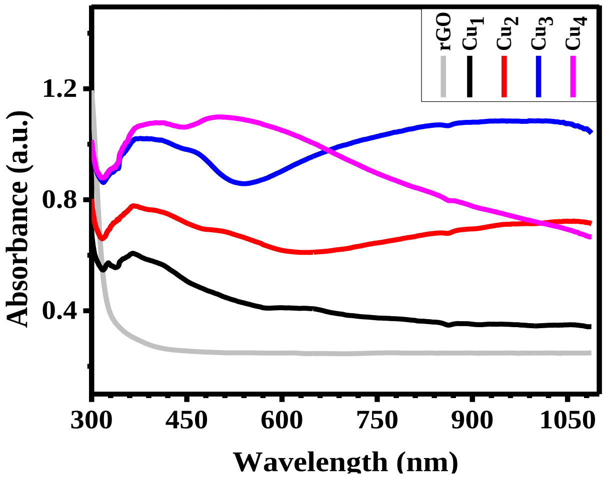

Figure 5. The UV-Vis absorbance spectra of reduced graphene and copper(I) oxide nanoparticles samples, i.e., rGO, Cu_1, Cu_2, Cu_3, and Cu_4.

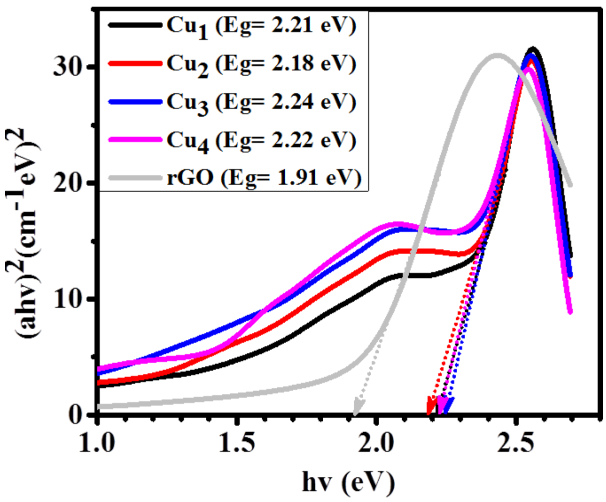

Figure 6. The energy band gap of Cu_2O NPs and rGO.

As can be seen in Fig 5, absorption spectrum of rGO showed that absorption peak of π to π* electronic transition of aromatic carbon appeared at wavelength lower than 300 nm (272 nm). Fig. 6 also shows that rGO a band gap of 1.91 eV which is lower than those of Cu_2O samples. Synthesizing composite with metal oxides semiconductors and rGO can lead to noticeable increase in efficiency of semiconductors. Such results are related to the high surface area of rGO for maximum adsorption and lesser electron-hole recombination which is a result of the higher conductivity offered by rGO sheets.

For all four Cu_2O samples, the absorbance gradually increased with the maximum peak in the visible light region, and the absorbance peaks of samples Cu_2 and Cu_3 suddenly decreased at about 600 nm. Then, these peaks reach a maximum value above 600 nm in the visible light region, and they also move to the UV region. Therefore, the size of Cu_2O nanoparticles increases with the increase in elongation, and the absorbance peak also increases but becomes straighter and shifts to the blue region of the spectrum. The shift of the absorbance peak from the higher (red) to the lower (blue) region indicates that the size of the nanoparticles is reduced. Therefore, the amount of NaOH strongly affects the size of the nanoparticles.

The added amount of NaOH affects the UV-Vis absorption spectrum of Cu_2O nanocrystals in different ways. The peak in the visible light region gradually increases and moves into the ultraviolet region. As a result, the experiment proves that the redshift is indulged in the blue region, which means that most of the cubic crystal has moved into the octahedron, and the lessons learned from this figure are retained, that is, the absorption of Cu_2O crystal shifts to blue and its elongation decreases/size dramatic increase. Therefore, XRD crystal size analysis and SEM size analysis confirmed the sizes of the four samples. These crystalline sizes are given in Table 2.

Visible Light-driven Photocatalytic Degradation of Bare Cu_2O NPs and Graphene-Based Composites of Cu_2O NPs

In the procedure of photocatalytic activity, Cu_2O has been used as a photocatalyst for the production of H_2 and usual pollutants degradation, under visible light exposure [30]. Previous analyses have revealed that the photocatalytic performance of Cu_2O is a high-class evaluation of morphology [31].

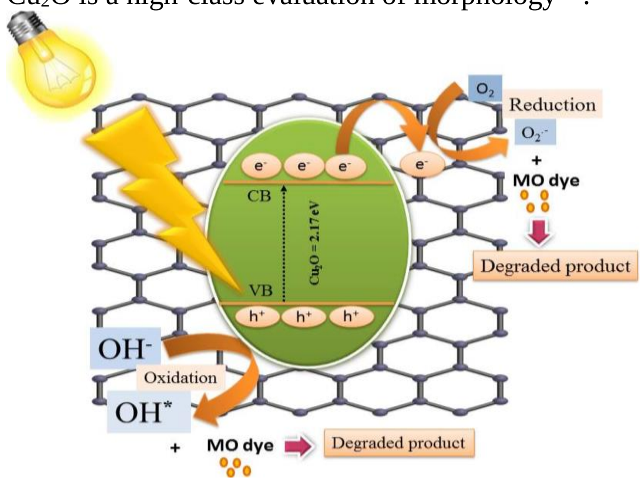

Figure 7. An illustration of the photocatalytic use of graphene nanosheets with Cu2O nanoparticles for Mo dyes

2023, 20(3 Suppl.): 1064 - 1077
https://dx.doi.org/10.21123/bsj.2023.8476
P-ISSN: 2078-8665 - E-ISSN: 2411-7986
Baghdad Science Journal

The photocatalytic performance of different bare CuO NPs and their composites with rGO was evaluated by the photodegradation of methylene orange under visible light irradiation. The first operation of the added amount of nanocatalyst in the degradation process is discussed [32]. When exposed to visible light, Cu_2O semiconductor oxide can be excited to generate electrons and most forms of holes [21]. These electrons and holes can initiate a chain of photodegradation processes. The pores in the valence band can oxidize the hydroxide ions adsorbed on the outside of the catalyst, thereby generating hydroxide ions that play an important role in photodegradation. On the contrary, the photogenerated electrons conducted by Cu from holes can be captured by absorbed O_2, and O_2 is initially generated (H_2O_2) and OH_2 or O_2 [33]. The O_2^- can additionally interact with H_2O_2 which simplifies the return of OH_2·OH and infield contributing to the photodegradation procedure of methyl orange [34]. In conclusion, methyl orange (MO) can be oxidized into intermediates. It can be absorbed from the surface of Cu_2O nanoparticles.

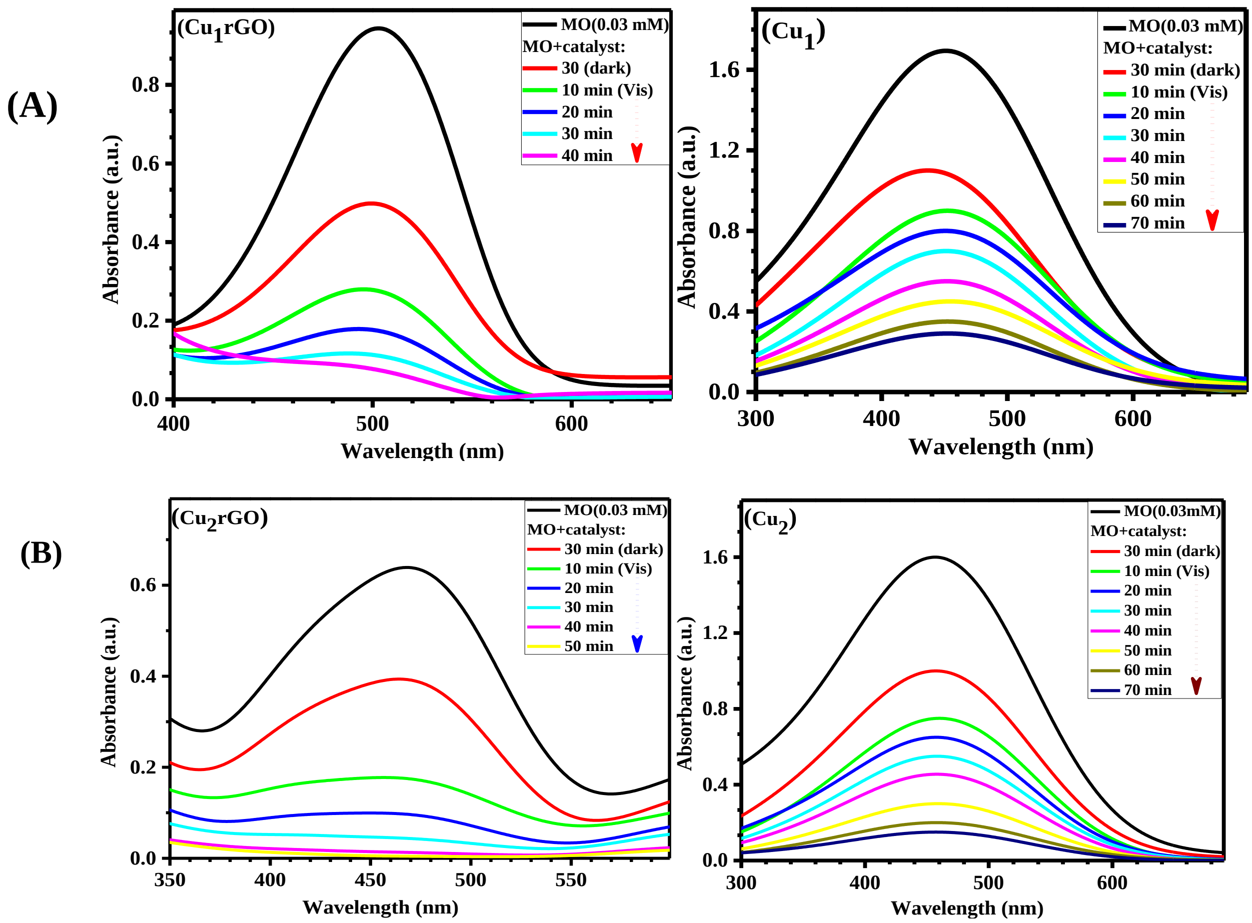

2023, 20(3 Suppl.): 1064 - 1077
https://dx.doi.org/10.21123/bsj.2023.8476
P-ISSN: 2078-8665 - E-ISSN: 2411-7986

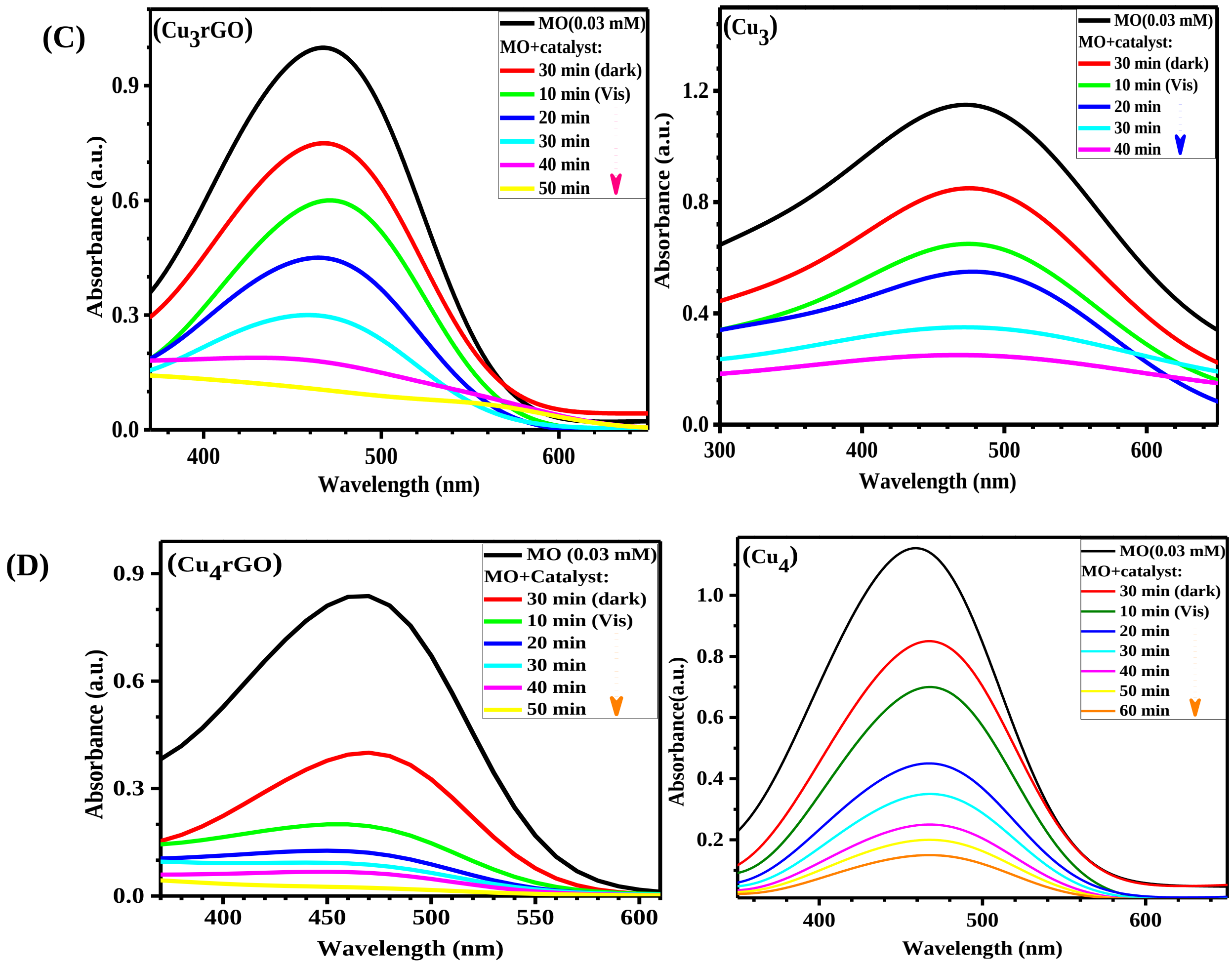

Figure 8. Comparisons through adsorption performance of different bare Cu_2O NPs and their composites with rGO for the degradation of MO in a photocatalytic process.

Fig 8 provides the photodegradation map of methylene orange and one observes the visual descriptive evaluation of photocatalysis of exposed Cu_2O NPs and rGO-based NPs. Fig 8A, is a comparative graphical representation of Cu_1 NPs and reduced graphene powder (Cu_1rGO) under the irradiation of a 200-watt visible light bulb. The first peak shows the absorbance at 451 nm, which is the peak of MO. After adding a catalyst consisting of a complex of bare and Cu_2O NPs, the figure shows the continuous degradation in the MO solution after each specific time interval (*i.e* 10 minutes), and the bare Cu_2O was recorded at 70 minutes degradation time of NPs, and the mixing time of graphene, pay attention to 40 minutes. It can be seen in Fig 8B, that the naked sample Cu_2 and the composite sample Cu_2rGO and MO dye solutions have the greatest degradation rate of all other samples. With the degradation of MO, the recording time for bare and composite materials was 70 minutes and 50 minutes, respectively. Fig 8C shows that compared with the bare sample Cu_3 and the composite sample Cu_3rGO, its crystallinity size is 14.85 nm. Compared with all other samples, the bare sample has less degradation at 40 minutes. Fig 8D shows the degradation process of sample Cu_4 and composite material sample Cu_4rGO with MO solution. The exposed sample time is 60 minutes, and the composite material sample's 50 minutes is the second-largest degradation time in the photocatalysis experiment. All four bare samples and composites of grapheme are examined bit by bit and upgraded with time increasing in a dark box with a hanging 200 Watt visible bulb. The reactant progress has been examined, and Cu_2 was observed with higher absorbance than that of the illustrative calculation of other Cu_2O NPs, which might survive recognized to (111) surfaces and are generally little sized. The photocatalytic decolonization of the methylene orange solution had been evaluated to completion at room temperature. One of them was the created sample, which contained reduced graphene powder and Cu_2O in a 2:1 ratio. Half of the

2023, 20(3 Suppl.): 1064 - 1077
https://dx.doi.org/10.21123/bsj.2023.8476
P-ISSN: 2078-8665 - E-ISSN: 2411-7986
Baghdad Science Journal

suspension, which was completely dissolved in 50 ml of methyl orange aqueous solution (0.03 mM), was used for photocatalytic testing. A visible light lamp with a 200 W output serves as the source of illumination. After 70/40 and 70/50 minutes, respectively, the time intervals required for the degradation processes of Cu_1/Cu_1/rGO and Cu_2/Cu_2rGO vanished. But following the elimination of the interval requirement, the Cu_3-Cu_3rGO and Cu_4-Cu_4rGO degradation processes were first observed after 40 to 50 and 60 to 50 minutes, respectively.

The Relationship between the Photodegradation Rate of Four Bare Samples and Reduced Graphene Powder on the Photocatalytic Degradation of MO and the Irradiation Time

In the photocatalytic process, it was observed that the sample Cu_2 has the highest adsorption capacity than other samples Cu_3, Cu_1, and Cu_4. That might be due to the nanoparticles size of sample Cu_2 which is smaller than other samples. The affiliation stuck between irradiation time along with photocatalytic degradation ratio of MO is exhibited in Fig 9. The photocatalytic degradation ratio is deliberate via using a first-order kinetic Equation (Eq. 2; $\boldsymbol{ln(A_0/A_t) = -kt}$)

- A_0 is the original absorbance of MO
- A_t is absorbance with a mixture of NPs at a certain time [35].

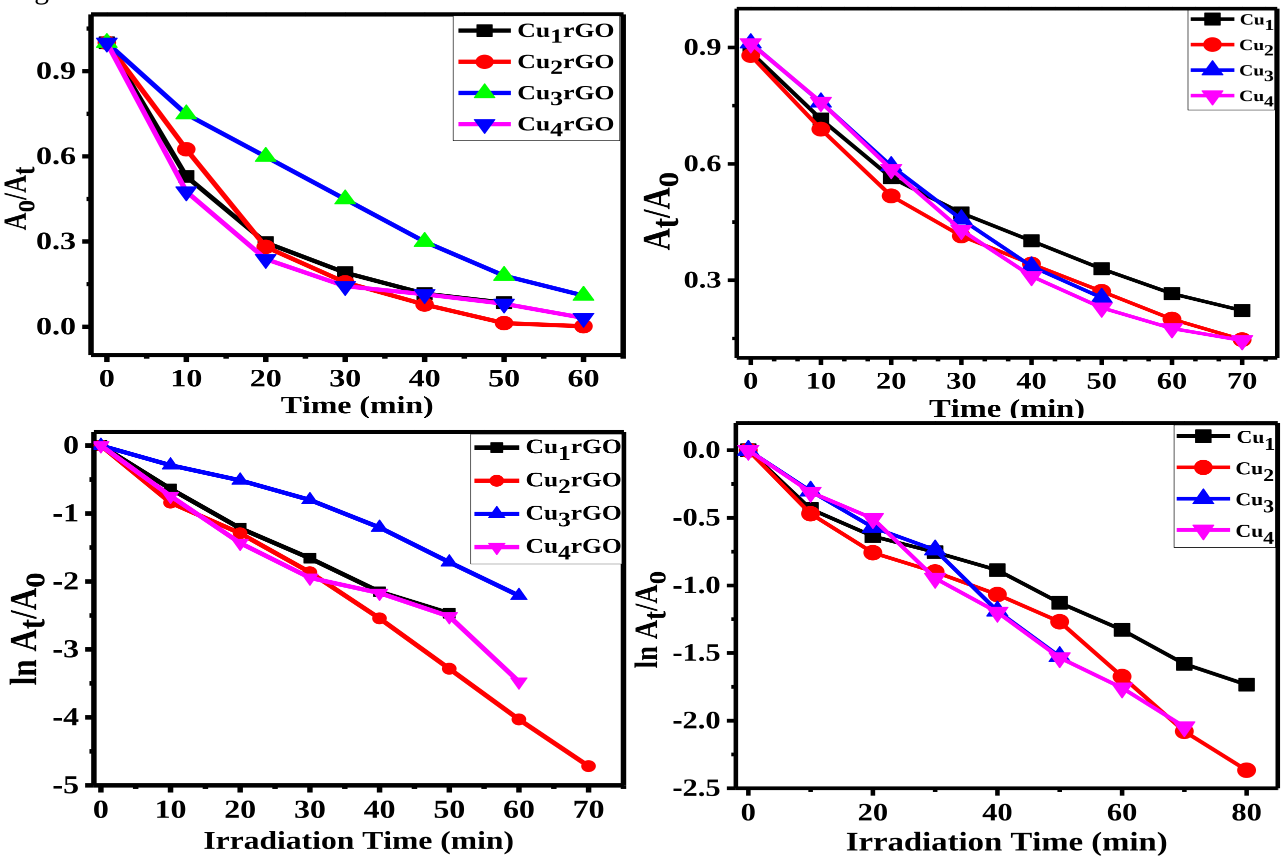

Figure 9. The stratagem of photodegradation ratio vs. irradiation time of samples for photocatalytic degradation of MO dye through Cu_2O nanoparticles and their rGO composites.

From Fig 9 and Eq 2, the degradation of methylene orange for all four Cu_1 to Cu_4 samples reached 82.35%, 90.01%, 78.26%, and 86.35%, respectively, thereby retaining the preserved visible light to promote the radiation of photocatalytic degradation. This indicates that Cu_2 has good photocatalytic performance under visible light irradiation, and MO is degraded. As the size of Cu_2O nanoparticles decreases, the time to reach MO decolourization decreases sharply [36]. Under the visible 200-watt bulb, a similar degradation process of graphene and Cu_2O NPs-based composites was also observed with MO dye. The reduced graphene and Cu_2O nanocomposite material shorten the irradiation time than bare samples. For the sample Cu_1rGO, the high efficiency is obtained after 40

2023, 20(3 Suppl.): 1064 - 1077
https://dx.doi.org/10.21123/bsj.2023.8476
P-ISSN: 2078-8665 - E-ISSN: 2411-7986
Baghdad Science Journal

minutes, which is 92.15%; for Cu_2rGO, the high efficiency is observed at 50 minutes, which is 99.08%, showing the largest degradation, compared with other studied photocatalysts. This may be due to their small sizes which were observed from SEM, compared to the other three samples. Graphite-like materials (graphene) can increase the surface charge of Cu_2O in the photocatalyst and inhibit the recombination of electron-hole pairs. The Cu_3rGO observed time for reaching the highest efficiency is 50 minutes, and the observed efficiency is 89.35%, which is due to the 10% increase of reduced graphene over bare Cu_1. Similarly, the degradation process of Cu_4rGO was repeated, the observed time was 50 minutes, and the observed degradation efficiency was 96.9%. It had the second smallest size, after Cu_2rGO, and it also had the second degradation efficiency, compared with other samples.

Table 3. The efficiency of NPs of Cu_2O/rGO with varying sizes and ratios of NPs.

Sr, No.	Bare Sample	Crystalline size (XRD) (nm)	Efficiency $D=[(A_0-A_t)/A_0]\times100\%$	Composites of rGO based Cu_2O NPs with (2:1)	Efficiency $D=[(A_0-A_t)/A_0]\times100\%$
1	Cu_1	13.01 nm	82.35%	Cu_1rGO	92.15%
2	Cu_2	11.66 nm	90.01%	Cu_2rGO	99.08%
3	Cu_3	14.27 nm	78.26%	Cu_3rGO	89.35%
4	Cu_4	12.29 nm	86.35%	Cu_4rGO	96.89%

Fig 9 shows the decolonization of methyl orange versus time observed by copper(I) oxide nanoparticles of different sizes. The samples (Cu_2-Cu_2rGO) and (Cu_4-Cu_4rGO) displayed high photocatalytic efficiency, compared to the remaining samples. The decrease in photocatalytic efficiency in Cu_3 may be attributed to the increase in the ratio of NaOH and the collection of Cu_2O particles. This is because the particle size has increased to micrometres, as mentioned earlier in Table 3.

Conclusion

A simplified wet chemical method was proposed to control structure during the synthesis of copper oxide (Cu_2O) nanoparticles (NPs). This can be achieved by adjusting the quantity of the ratio of deionized water and sodium hydroxide in the mixed aqueous solution. The crystal sizes of Cu_2O NPs required for the measurement are Cu_1/13.006 nm, Cu_2/11.66 nm, Cu_3/14.85 nm, and Cu_4/12.35 nm, respectively. The structure and optical properties of copper(I) oxide are obtained by X-ray diffraction and UV-Vis spectroscopy. Methyl orange (MO) dye was selected as the probe molecule to evaluate the photocatalytic activity of four exposed Cu_2O NPs and reduced graphene samples just used under 200 watts of visible light. Experiments showed that the use of a composite material of bare and reduced graphene can more effectively degrade MO in the mixed aqueous solution. The photocatalytic decolourization of MO in an aqueous Cu_2O suspension based on bare and reduced graphene composites was carried out by UV-VIS spectroscopy to study the photocatalytic behaviour of Cu_2O NPs with various crystal sizes. Under visible light, the absorption of all bare copper(I) nanoparticles was observed, and the decolourization efficiency of the MO solution reached by the bare Cu_2O NP was 82.35%, 90.01%, 78.26%, 86.35%, and 81.80%, respectively. However, it was observed that the absorption of all reduced graphene alloy-based copper(I) oxides reduced the time, and the highest efficiency reached 92.15%, 99.08%, 89.35%, 96.89%, and 91.9%, respectively. These results showed that the efficiency of the sample number (Cu_2-Cu_2rGO) has a higher performance both in the case of bare and rGO composites, but the sample (Cu_3-Cu_3rGO) has a lower absorption rate than the other samples. The photocatalytic results showed that copper(I) NPs produced with 0.25 mL NaOH (1.0 M) were the best sample during preparation. Because it has good light harvesting ability, and both in the bare sample and in the composite forms it has the highest MO solution decolourization efficiency, respectively in 70 minutes and 50 minutes. Therefore, the composition of Cu_2O/graphene photocatalyst may be a potential choice for using solar energy to purify wastewater and remove pollutants (especially emerging pollutants).

Acknowledgment

Sincere thanks to Dr Hadi Sajid Abdulabbas for his help in editing the Arabic abstract.

Author's Declaration

- Conflicts of Interest: None.
- We hereby confirm that all the Figures and Tables in the manuscript are ours. Furthermore, any Figures and images that are not ours have been included with the necessary permission for re-publication, which is attached to the manuscript.
- Authors sign on ethical consideration's approval.
- Ethical Clearance: Not applicable; there was no need for the project to be approved by any ethical committee, since it was not engaged with human or animals.

Author Contribution Statement

A W R: Conceptualization, Investigation, Data curation, Writing-original draft, Writing-Reviewing and Editing; G N: Writing-original draft, Writing-Reviewing and Editing; E B: Writing-Reviewing and Editing; B L: Writing-Reviewing and Editing; A B S: Writing-Reviewing and Editing; A H-B: Conceptualization, Data modeling; Writing-Reviewing and Editing. All authors have read and approved the manuscript.

References

1. Stroea L, Buruiana T, Buruiana E C. Synthesis and solution properties of thermosensitive hydrophilic imidazole-based copolymers with improved catalytic activity. Mater Chem Phys. 2019; 223: 311-318. https://doi.org/10.1016/j.matchemphys.2018.10.066
2. Suleiman M, Mousa M, Hussein A, Hammouti B; Hadda T B; Warad I. Copper (II)-oxide nanostructures: synthesis, characterizations and their applications-review. J Mater Environ Sci. 2013; 4 (5): 792-797.
3. Lan T, Fallatah A, Suiter E, Padalkar S. Size controlled copper (I) oxide nanoparticles influence sensitivity of glucose biosensor. Sensors 2017; 17 (9): 1944. https://doi.org/10.3390/s17091944
4. Chen L-C. Review of preparation and optoelectronic characteristics of Cu2O-based solar cells with nanostructure. Mater Sci Semicond Process. 2013; 16 (5): 1172-1185. https://doi.org/10.1016/j.mssp.2012.12.028
5. Su Y, Li H, Ma H, Robertson J, Nathan A. Controlling surface termination and facet orientation in Cu2O nanoparticles for high photocatalytic activity: a combined experimental and density functional theory study. ACS Appl Mater Interfaces 2017; 9 (9): 8100-8106. https://doi.org/10.1021/acsami.6b15648
6. Mehra P, Lamberts B, Chatradhi S, Katine J A. Embedded disconnected circuits in magnetic storage media of data storage devices. Google Patents: 2020.
7. Lu T-F, Li W, Chen J, Tang J, Bai F-Q, Zhang H-X. Promising pyridinium ylide based anchors towards high-efficiency dyes for dye-sensitized solar cells applications: Insights from theoretical investigations. Electrochim Acta. 2018; 283: 1798-1805. https://doi.org/10.1016/j.electacta.2018.07.108
8. Chiu Y-H, Chang T-F M, Chen C-Y, Sone M, Hsu Y-J. Mechanistic insights into photodegradation of organic dyes using heterostructure photocatalysts. Catalysts. 2019; 9 (5): 430.
9. Ren Y, He X, Sui W, Zhang L, Zhang H, Xia Y et al. Carbon/binder free 3D Si@ Cu2O anode for high performance lithium ion battery. J Mater Res Technol. 2020; 9 (4): 8081-8091. https://doi.org/10.1016/j.jmrt.2020.05.086
10. Zhang R, Liu X, Zhou T, Zhang T. Controllable construction of multishelled p-type cuprous oxide with enhanced formaldehyde sensing. J Colloid Interface Sci. 2019; 535: 58-65. https://doi.org/10.1016/j.jcis.2018.09.081
11. Gawande M B, Goswami A, Felpin F-X, Asefa T, Huang X, Silva R et al. Cu and Cu-based nanoparticles: synthesis and applications in catalysis. Chem Rev. 2016; 116 (6): 3722-3811. https://doi.org/10.1021/acs.chemrev.5b00482
12. Ibrahim IM, Salman MO, Ahmed AS. Electrical behavior and Optical Properties of Copper oxide thin Films. Baghdad Sci J. 2011; 8(2): 638-645. https://doi.org/10.21123/bsj.2011.8.2.638-645

13. Hassan A K, Atiya M A, Luaibi I M. A Green Synthesis of Iron/Copper Nanoparticles as a Catalytic of Fenton-like Reactions for Removal of Orange G Dye. Baghdad Sci J. 2022; 19 (6): 1249. https://doi.org/10.21123/bsj.2022.6508
14. Naz G, Shamsuddin M, Butt F K, Bajwa S Z, Khan W S, Irfan M et al. Au/Cu2O core/shell nanostructures with efficient photoresponses. Chinese J Phys. 2019; 59: 307-316. https://doi.org/10.1016/j.cjph.2019.03.008
15. Yeh T F, Teng C Y, Chen S J, Teng H. Nitrogen-doped graphene oxide quantum dots as photocatalysts for overall water-splitting under visible light Illumination. Adv Mater. 2014; 26 (20): 3297-3303. https://doi.org/10.1002/adma.201305299
16. Huang H, Zhang J, Jiang L, Zang Z. Preparation of cubic Cu2O nanoparticles wrapped by reduced graphene oxide for the efficient removal of rhodamine B. J Alloys Compd. 2017; 718: 112-115. https://doi.org/10.1016/j.jallcom.2017.05.132
17. Larm N E, Essner J B, Pokpas K, Canon J A, Jahed N, Iwuoha E I et al. Room-temperature turkevich method: formation of gold nanoparticles at the speed of mixing using cyclic oxocarbon reducing agents. J Phys Chem C 2018; 122 (9): 5105-5118. https://doi.org/10.1021/acs.jpcc.7b10536
18. Fang S, Bresser D, Passerini S. Transition metal oxide anodes for electrochemical energy storage in lithium- and sodium-ion batteries. Adv Energy Mater. 2020; 10 (1): 1902485 https://doiorg/101002/9783527817252ch4
19. Hu Z, Mi Y, Ji Y, Wang R, Zhou W, Qiu X et al. Multiplasmon modes for enhancing the photocatalytic activity of Au/Ag/Cu 2 O core–shell nanorods. Nanoscale 2019; 11 (35): 16445-16454. https://doiorg/101039/C9NR03943K
20. Sachin S S, Ashok D B, Chandrashekhar M M Synthesis of cuprous oxide (Cu2O) nanoparticles–a review. J Nano-Electron**. 2016**; (8, 1): 01035. https://doiorg/1021272/jnep8(1)01035
21. Wei B, Yang N, Pang F, Ge J Cu2O–CuO Hollow Nanospheres as a Heterogeneous Catalyst for Synergetic Oxidation of CO. J Phys Chem C. 2018; 122 (34): 19524-19531. https://doiorg/101021/acsjpcc8b04690
22. Kumar S, Ojha A K, Bhorolua D, Das J, Kumar A, Hazarika A Facile synthesis of CuO nanowires and Cu2O nanospheres grown on rGO surface and exploiting its photocatalytic, antibacterial and supercapacitive properties. Physica B Condens Matter. 2019; 558: 74-81. https://doiorg/101016/jphysb201901040
23. Kang Z, Liu Y Catalytic applications of carbon dots In Carbon Nanoparticles and Nanostructures, Springer, 2016: 257-298. https://doiorg/101007/978-3-319-28782-9_8
24. Kumar R, Sudhaik A, Raizada P, Hosseini-Bandegharaei A, Thakur VK, Saini A et al. An overview on bismuth molybdate based photocatalytic systems: Controlled morphology and enhancement strategies for photocatalytic water purification. J Environ Chem Eng. 2020; 8(5): 104291. https://doiorg/101016/jjece2020104291
25.Wu W, Jiang C Z, Roy V A Designed synthesis and surface engineering strategies of magnetic iron oxide nanoparticles for biomedical applications. Nanoscale. 2016; 8 (47): 19421-19474. https://doiorg/101039/C6NR07542H
26. Sui Y, Zeng Y, Fu L, Zheng W, Li D, Liu B, Zou B. Low-temperature synthesis of porous hollow structured Cu2O for photocatalytic activity and gas sensor application. RSC Adv. 2013; 3 (40): 18651-18660. https://doiorg/101039/C3RA42192A
27. Zhou Z, Li X, Li Q, Zhao Y, Pang H. Copper-based materials as highly active electrocatalysts for the oxygen evolution reaction Mater Today Chem. 2019; 11: 169-196. https://doiorg/101016/jmtchem201810008
28. Munawar T, Mukhtar F, Nadeem M S, Mahmood K, Hussain A, Ali A et al. Structural, optical, electrical, and morphological studies of rGO anchored direct dual-Z-scheme ZnO-Sm2O3–Y2O3 heterostructured nanocomposite: An efficient photocatalyst under sunlight. Solid State Sci. 2020; 106: 106307. https://doiorg/101016/jsolidstatesciences2020106307
29. Sakthivel S, Kisch H. Daylight photocatalysis by carbon-modified titanium dioxide. Angew Chem Int Ed. 2003; 42 (40): 4908-4911. https://doiorg/101002/anie200351577
30. Chen W-T, Dosado A G, Chan A, Sun-Waterhouse D, Waterhouse G I. Highly reactive anatase nanorod photocatalysts synthesized by calcination of hydrogen titanate nanotubes: Effect of calcination conditions on photocatalytic performance for aqueous dye degradation and H2 production in alcohol-water mixtures. Appl Catal A-Gen. 2018; 565: 98-118. https://doiorg/101016/japcata201808004
31. Yue Y, Zhang P, Wang W, Cai Y, Tan F, Wang X et al. Enhanced dark adsorption and visible-light-driven photocatalytic properties of narrower-band-gap Cu2S decorated Cu2O nanocomposites for efficient removal of organic pollutants. J Hazard Mater. 2020; 384: 121302. https://doiorg/101016/jjhazmat2019121302
32. Kavitha S, Jayamani N, Barathi D A. study on preparation of unique TiO2/Cu2O nanocomposite with highly efficient photocatalytic reactivity under visible-light irradiation. Mater Technol. 2021; 36(11): 670-683. https://doiorg/101080/1066785720201786785
33. Liao W, Liu X, Yang Y, Du M. Relationship and mechanism between microstructure and property of C70250 copper alloy strip prepared by temperature controlled mold continuous casting. Mater Sci Eng A. 2019; 767: 138428. https://doiorg/101016/jmsea2019138428
34. Kang N Design, Synthesis, and Characterization of Nanostructured Materials for Energy Storage Devices

and Flexible Chemical Sensors State University of New York at Binghamton, 2017.
35 Zhang X, Song J, Jiao J, Mei X. Preparation and photocatalytic activity of cuprous oxides. Solid State Sci. 2010; 12 (7): 1215-1219. https://doiorg/101016/jsolidstatesciences201003009
36. Mikami K, Kido Y, Akaishi Y, Quitain A, Kida T. Synthesis of Cu_2O/CuO Nanocrystals and their application to H_2S sensing. Sensors (Basel) 2019; 19 (1): 211. https://doiorg/103390/s19010211

الخواص التحفيزية الضوئية المرئية لأكسيد النحاس (الأول) ومركباته النانوية المعتمدة على الجرافين

عبد الوحيد رباني[1]، جل ناز[1]، اليور برديمرادوف[2]، باسنت لال[3]، آيقول بايمقامبتووا سايلواونا[4] و أحمد حسيني بنده قرائى[5]

[1]معهد الفيزياء ، الجامعة الإسلامية باهاوالبور ، بهاولبور 63100 ، باكستان.
[2]كلية الكيمياء ، جامعة أوزبكستان الوطنية ، طشقند ، أوزبكستان.
[3]قسم الكيمياء ، معهد العلوم التطبيقية والإنسانية ، جامعة GLA ، ماثورا 281406 ، الهند.
[4]معهد العلوم الطبيعية والجغرافيا ، جامعة آباي ، ألماتي 050010 ، كازاخستان.
[5] كلية الكيمياء ، جامعة سمنان ، سمنان ، إيران.

الخلاصة

في هذه الدراسة، تم اقتراح طريقة مطورة لتخليق جزيئات أكسيد النحاس (الأول) (Cu_2O) النانوية ذات تراكيب محكمة، باستخدام طريقة كيميائية مبسطة وظروف رطبة في درجة حرارة الغرفة. حيث تم استخدام محلول كيميائي لتجميع بلورات أكسيد النحاس (الأول) Cu_2O بأحجام وأشكال مختلفة. اضافة الى دراسة التركيب والشكل والخصائص الضوئية لجسيمات أكسيد النحاس النانوية بواسطة حيود الأشعة السينية والمجهر الإلكتروني الماسح (SEM) والتحليل الطيفي للأشعة المرئية وفوق البنفسجية. ومن خلال معادلة محاليل الخليط المائي لهيدروكسيد الصوديوم (NaOH) وكلوريد هيدروكسيل الأمونيوم ($NH_2OH \cdot HCl$) يمكن تخليق بلورات أكسيد النحاس (الأول) (Cu_2O) بشكل وحجم مختلفين. وقد وجد أن التغير في نسبة الماء غير المتأين ومحلول هيدروكسيد الصوديوم المائي يؤدي إلى تكوين بلورات أكسيد النحاس (الأول) بأحجام مختلفة، بينما لم يتأثر شكل هذه البلورات. بعدها استخدمت بلورات أكسيد النحاس (الأول)المُصنَّعة كمحفزات ضوئية نموذجية لتحلل صبغة الميثيل البرتقالي (MO) لتقييم أنشطة التحفيز الضوئي. وعلى أي حال، تحت 200 واط من مصدر ضوء مرئي، هناك أربع عينات مع وبدون مركبات نانوية من النحاس تعتمد على الجرافين (NPs). كما أظهرت نتائج المقارنة مع الصفائح الكروية غير المنتظمة شبه السميكة، فإن جزيئات أكسيد النحاس (الأول) النانوية المتمثلة بكرات الطوب والحبيبات الصغيرة اظهرت نشاطًا أفضل. أظهرت عينة أكسيد النحاس (الأول) ذات الأشكال غير المنتظمة والتي تشبه الصفائح الدموية السميكة الحاوية على جسيم متوسط حجمه 0.53 مايكرومتر نشاطًا تحفيزيًا ضوئيًا ممتازًا. بالإضافة إلى ذلك، من خلال تقليل حجم جزيئات أكسيد النحاس (الأول) وتحضير تركيبة مختلفة (Cu_2-Cu_2Gr)، يمكن تصنيع عينة بأعلى كفاءة وذات نشاط تحفيزي ضوئي أفضل بشكل ملحوظ مقارنة بالجزيئات الاخرى. يمثل هذا البحث استراتيجية مبتكرة للإنتاج المسبق للمواد النانوية ذات الأشكال والأحجام كبلورات أكسيد النحاس (الأول) ذات نشاط تحفيزي ضوئي ممتاز من خلال تصنيعها باستخدام الجرافين.

الكلمات المفتاحية: أكسيد النحاس (الأول) ، المركبات النانوية القائمة على الجرافين، بلورات النانو تقييم ضوئي، ضوء مرئي.